Proceedings of the Conference on Computational Engineering and Science JSCES
Vol. 30, Jun. 2025

Sequential Updating of Building Fragility Functions through City-Scale Seismic Simulations and Sensor Integration

Dongyang Tang[1], Naruethep Sukulthanasorn[2], Reika Nomura[2], Kazuya Nojima[3], Atsushi Mori[3], Susumu Ohno[4], Jia Guo[5], Seiichi Sato[3], Shuji Moriguchi[4], Masaaki Sakuraba[3] and Kenjiro Terada[6]

[1] Graduate student (Civil and Environmental Engineering, Tohoku University, 980-0845, Sendai, Japan, E-mail: tang.dongyang.r3@dc.tohoku.ac.jp)
[2] Assistant Professor (International Research Institute of Disaster Science, Tohoku University, 980-0845, Sendai, Japan)
[3] Nippon Koei Co., Ltd. (Inarihara 2304, Tsukuba, Ibaraki, 300-1259, Japan)
[4] Associate Professor (International Research Institute of Disaster Science, Tohoku University, 980-0845, Sendai, Japan)
[5] Associate Professor (Division of Environmental Science and Technology, Kyoto University, 606-8502, Kyoto, Japan)
[6] Professor (Department of Civil and Environmental Engineering, Tohoku University, 980-8579, Sendai, Japan)

This study proposes a framework for assessing the seismic risk of buildings in large-scale urban areas. City-scale numerical simulations and sensor networks are integrated to update building-specific fragility functions. The proper orthogonal decomposition (POD) technique plays a crucial role in analyzing numerical simulation data. The POD-based approach helps to represent large-scale simulation results in a more compact and meaningful way, a crucial step in understanding seismic impacts. The framework also highlights the importance of sparse sensor distribution. Furthermore, this study uses cloud analysis and Bayesian updating to update the fragility functions of buildings based on sensor data. Fragility functions for all buildings are created based on cloud analysis using numerical simulation data, and then progressively refines them by incorporating sensor data through Bayesian inference. This dual-stage approach allows for a rapid risk assessment of all buildings in a target area, with continuous improvements to fragility functions by the sensor data.

Key Words : *Seismic Risk Assessment, Numerical simulation, Proper orthogonal decomposition, Sparse sensing, Fragility Function*

1. Introduction

Earthquakes pose a significant threat to urban areas, challenging city resilience and complicating risk prediction and assessment. Powerful earthquakes such as the 2011 eastern Japan earthquake and the 2023 Turkey–Syria earthquake have caused extensive casualties and significant losses. This study proposes a framework for assessing the seismic risk of buildings in large-scale urban areas, which integrates city-scale numerical simulations and a sparse sensor network. The key aspect of this approach is the use of numerical simulation to create fragility functions for each building, and to identify efficient sensor distribution. Furthermore, the data obtained from the sensors are used to update the fragility functions, progressively enhancing their accuracy and providing a more precise assessment of seismic impacts on urban structures.

A crucial aspect of this study is the application of the proper orthogonal decomposition (POD) to analyze numerical simulation data. POD can identify principal components from numerical simulation data, enabling effective data decomposition and reconstruction. This approach enables a more compact and meaningful representation of numerical simulation results, which is crucial for understanding seismic impacts. Additionally, the framework also highlights the importance of sparse sensor distribution. The framework strategically places sensors to maximize data collection efficiency while minimizing the number of sensors. This optimization isessential for practical applications in urban areas, where large sensor networks may be impractical.

The fragility functions for all buildings are created using simulation data based on the concept of the cloud analysis. Cloud analysis uses the linear regression in the logarithmic scale by least squares to establish the relationship between engineering demand parameter (EDP) and intensity measure (IM). Obtained fragility functions are then updated using the sensor data based on Bayesian inference. This update improves the accuracy and realism of the fragility functions.

In this study, a trial calculation is finally conducted to verify the effectiveness of the proposed framework, focusing on Sendai City as the target area.

2. Numerical simulation

The following two methods were employed to calculate the propagation of seismic waves from the fault to

the ground surface and the response of buildings on the ground.

(1) Stochastic Green's Function

The Stochastic Green's function method builds upon the empirical Green's function method, which was introduced by Irikura[2]. The empirical Green's function method relies on observed records as Green's functions, assuming that the deep and shallow subsurface structures at the observation point are already integrated into the observed records. On the other hand, this method serves as an effective alternative when appropriate observation records cannot be obtained.

In the application of the Stochastic Green's function method by Dan and Sato[3], the fault surface is segmented into small sub-faults, and Boore's stochastic source model is taken into account for each sub-fault to compute the Green's functions. The deep subsurface structure is treated as a one-dimensional layered structure for ground response analysis. Random phase characteristics are attributed to this Green's function, and waveform synthesis is conducted by Irikura[2] to derive the seismic waveforms when the entire fault experiences rupture. This study utilizes the program provided by the National Research Institute for Earth Science and Disaster Resilience[3].

(2) Integrated Earthquake Simulator(IES)

IES is a program that is linked to a Geographic Information System (GIS) and incorporates earthquake motion simulation, structural response simulation, and response behavior simulation[5].

Wave propagation simulation: It outputs synthesized earthquake waves based on the fault mechanism. The propagation of waves passing through the crust is calculated, and the amplification of waves near the surface is calculated taking into account the non-linear characteristics of the 3-dimensional topographical effect and the shallow soil layer.

Structural response simulation: It calculates the response for all structures in the targeted area, including residential buildings, concrete infrastructure structures, geological structures, transportation networks, etc. It is necessary to choose an appropriate analysis method depending on the structure of the building.

Response behavior simulation: It is possible to analyze evacuation from building damage, crisis management, and restoration plans.

Finally, by modifying the fault model, multiple scenarios were generated, and using both the Stochastic Green's Function and IES, training and validation datasets were computed.

3. Sparse sensor distribution

The first part of this framework is a prediction model, based on POD and sparse sensing, it can predict both seismic motion and structure response in a large area.

POD is mathematical operation that can extract modes from original data, allowing for mode decomposition based on the theory of singular value decomposition[6]. Let $\boldsymbol{x}_i$ represent the n-dimensional simulation result for a specific case i, and define the data $\boldsymbol{X}$ by arranging N cases in a row direction.

By applying singular value decomposition of $\mathbf{X}$ as follows:

$$\boldsymbol{X} = \boldsymbol{U}\boldsymbol{\Sigma}\boldsymbol{V}^T \tag{1}$$

By retaining only r columns from the r singular values and their corresponding modes $\boldsymbol{U}$(left singular vector), we obtain an $n \times r$ matrix. Similarly, by retaining only r columns from the singular vector matrix $\boldsymbol{V}$, we obtain an $N \times r$ matrix. $\boldsymbol{x}$ as follows:

$$\boldsymbol{X} = \boldsymbol{U}_r\boldsymbol{\Sigma}_r\boldsymbol{V}_r^T = \sum_{k=1}^{r} \boldsymbol{u}_k(\sigma_k \boldsymbol{v}_k^T), \tag{2}$$

in which

$$\boldsymbol{x}_i = \sum_{j=1}^{N} (\sigma_j v_{ij}^T)\boldsymbol{u}_j = \sum_{j=1}^{N} z_{ij}\boldsymbol{u}_j. \tag{3}$$

Here σ_k represents the k-th singular value, and v_{ik} represents the i-th component of $\boldsymbol{V}$ in the k-th column. Thus, the data x_i for a specific case i is given by the sum of the products of the singular values, the i-th component of $\boldsymbol{U}$, and the i-th component of $\boldsymbol{V}$, for k ranging from 1 to r.

Then we consider the following linear system:

$$\boldsymbol{y} = \boldsymbol{H}\boldsymbol{U}\boldsymbol{z} = \boldsymbol{C}\boldsymbol{z}. \tag{4}$$

The equation describes a system where $\boldsymbol{y} \in \mathrm{R}^p$ is the observation vector, $\boldsymbol{H} \in \mathrm{R}^{p \times n}$ represents the sparse sensor location matrix, $\boldsymbol{U} \in \mathrm{R}^{n \times r}$ denotes the sensor candidate matrix, $z \in \mathrm{R}^r$ is the latent state vector, and $\boldsymbol{C} \in \mathrm{R}^{p \times r}$ is the measurement matrix, with $\boldsymbol{C} = \boldsymbol{H}\boldsymbol{U}$ being their relation. In the matrix $\boldsymbol{H}$, each row has a unity element indicating the sensor location, with all other elements being zero. When observations are subjected to uniform independent Gaussian noise, represented as $N(0, \sigma^2\boldsymbol{I})$, the estimated parameters $\hat{z}$ are derived applying a pseudo-inverse method as

$$\hat{\boldsymbol{z}} = \begin{cases} \boldsymbol{C}^T(\boldsymbol{C}\boldsymbol{C}^T)^{-1}\boldsymbol{y}, & p \le r, \\ (\boldsymbol{C}^T\boldsymbol{C})^{-1}\boldsymbol{C}^T\boldsymbol{y}, & p > r. \end{cases} \tag{5}$$
$$\text{subject to } \boldsymbol{C} \in \mathrm{R}^{p \times r},\ p, r \in \mathrm{N}.$$

A D-optimal design aims to minimize the determinant of the error covariance matrix. This can also be seen to minimize the determinant of the error covariance matrix.

$$\max f_D, \quad f_D = \begin{cases} \det\left(\boldsymbol{C}\boldsymbol{C}^{\boldsymbol{T}}\right) & (p \le r) \\ \det\left(\boldsymbol{C}^{\boldsymbol{T}}\boldsymbol{C}\right) & (p > r) \end{cases} \tag{6}$$

To maximaze the objective function, genetic algorithm is adopted in this study.

4. Sequential city scale risk assessment

Despite the fact that the global prediction can be achieved by the sparse sensor network in the preceding section, this sparsity inevitably introduces observation errors at local observation points. Consequently, for a specific building, the arrival of continuous prediction observations directly affects the subsequent risk assessment due to the accumulation of noise. In order to address these errors and further enable detailed risk assessments at the building level, this chapter introduces a hierarchical modeling approach to develop a risk assessment framework.

(1) Cloud analysis

Fragility functions are derived from a structural assessment of the system (in the case of analytical form). In simpler terms, fragility can be defined as the susceptibility of a structure to collapse or being damaged. It is a continuous function showing the probability of exceeding a certain limit state (LS) for a specific level of ground motion intensity measure (IM)[8] as blow

$$Fragility = P[LS|IM = im] \tag{7}$$

Cloud analysis uses the linear regression in the logarithmic scale to establish the relationship between engineering demand parameter (EDP) and IM. The fragility function is expressed as the damage probability that EDP exceeds the pre-defined threshold for each limit state (LS) conditional on IM. This probability can be derived based on the above linear relationship between EDP and IM under the lognormal probability distribution[9] as

$$\begin{aligned} &P_f[EDP \geq LS \mid IM, \eta, b] \\ &= \Phi\left\{\frac{\ln(\mu_d) - \ln(LS)}{\sigma_d}\right\} = \Phi\left\{\frac{\ln(IM) - \ln(\eta)}{b}\right\}, \end{aligned} \tag{8}$$

where $\Phi(\cdot)$ is standard normal cumulative distribution function (CDF); η is median of the fragility function, i.e, $\ln(\eta) = [\ln(LS) - \ln(a)]/b$; and b is dispersion of the fragility function, i.e., $b = \sigma_d/b$.

Limit state refers to a specific level of damage or failure that is used to define fragility functions. In this case, the limit states of "moderate" was chosen from HAZUS[12] to develop the fragility functions.

(2) Bayesian hierarchical city-scale fragility modeling

Given that the fragility function is derived by cloud analysis for each building's observed intensity measure and engineering demand parameter, our focus on such a regression problem necessitates the definition of a hierarchical modeling[13][14] that enables data pooling (sharing) between buildings of the same type, as shown in Fig.1. This reduces the deviation from the risk model due to the accumulation of predicted noise in individual buildings. The proposed approach involves a greedy algorithm for updating the fragility risk assessment model, which is incrementally enhanced by adding observations. This approach is more sustainable than database updates and does not result

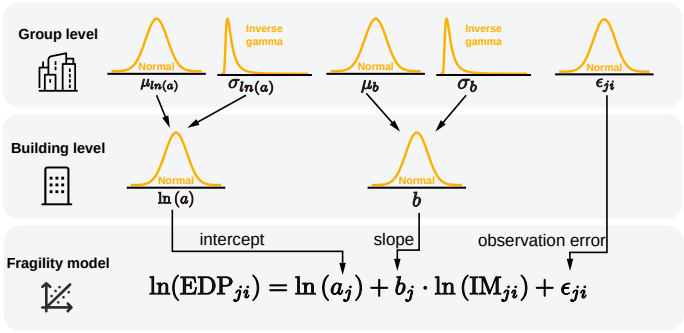

Fig. 1 Bayesian hierarchical modeling

in the accumulation of computational and storage efficiencies due to data buildup.

Assuming that each building has a regression problem for the IM-EDP in the log domain, as illustrated in the figure, each building can compute the respective regression coefficients under the specified normal distribution for the respective predicted IM-EDP data, that is, the building level in the figure. Subsequently, a layer of group level, that is, the hyper-parameter layer, has been established. The pooling of regression coefficients among individuals isachieved, meaning that individual data must refer to the mean of the global regression coefficients to a certain extent, which also ensures that the data of some buildings with excessive prediction errors is pulled back to the mean.

For each building j and observation i, we assume:

$$\ln(EDP_{j,i}) = \ln(a)_j + b_j \ln(IM)_{j,i} + \varepsilon_{j,i}, \quad \varepsilon_{j,i} \sim \mathcal{N}(0, \sigma^2).$$

Regression parameters are assigned:

$$\ln(a)_j \sim \mathcal{N}(\mu_{\ln(a)}, \sigma^2_{\ln(a)}), \quad b_j \sim \mathcal{N}(\mu_b, \sigma^2_b), \tag{9}$$

with global parameters given by

$$\mu_{\ln(a)} \sim \mathcal{N}(\theta_{\mu_{\ln(a)}}, \tau^2_{\mu_{\ln(a)}}), \quad \mu_b \sim \mathcal{N}(\theta_{\mu_b}, \tau^2_{\mu_b}). \tag{10}$$

Variance parameters σ^2, $\sigma^2_{\ln(a)}$, and σ^2_b are modeled on the log-scale to ensure positivity. The complete joint probability is:

$$\begin{aligned} p(\theta, \boldsymbol{D}) = {} & p(\mu_{\ln(a)})\, p(\mu_b)\, p(\sigma^2_{\ln(a)})\, p(\sigma^2_b)\, p(\sigma^2) \\ & \times \prod_{j=1}^{J} \Big\{ p(\ln(a)_j \mid \mu_{\ln(a)}, \sigma^2_{\ln(a)})\, p(b_j \mid \mu_b, \sigma^2_b) \\ & \times \prod_{i=1}^{I} p(\ln(EDP)_{j,i} \mid \ln(a)_j, b_j, \ln(IM)_{j,i}, \sigma^2) \Big\}. \end{aligned} \tag{11}$$

To approximate the posterior $p(\theta \mid y)$, we use a mean-field variational distribution[15][16]:

$$\begin{aligned} q(\theta) = {} & q(\mu_{\ln(a)})\, q(\mu_b)\, q(\sigma^2_{\ln(a)})\, q(\sigma^2_b)\, q(\sigma^2) \\ & \times \prod_{j=1}^{J} q(\ln(a)_j)\, q(b_j), \end{aligned} \tag{12}$$

The individual factors are parameterized as follows:

$$q(\mu_\alpha) = \mathcal{N}\Big(m_{\mu_\alpha},\, s^2_{\mu_\alpha}\Big), \quad q(\mu_\beta) = \mathcal{N}\Big(m_{\mu_\beta},\, s^2_{\mu_\beta}\Big). \tag{13}$$

A sample is obtained via the reparameterization:

$$\mu_\alpha = m_{\mu_\alpha} + s_{\mu_\alpha}\,\varepsilon_{\mu_\alpha}, \quad \varepsilon_{\mu_\alpha} \sim \mathcal{N}(0,1), \tag{14}$$

and similarly for μ_β. To ensure positivity, operate in the log domain as below.

$$u_\alpha = \log\sigma^2_\alpha, \quad u_\beta = \log\sigma^2_\beta, \quad u = \log\sigma^2. \tag{15}$$

Then,

$$\begin{aligned} u_\alpha &\sim \mathcal{N}\Big(m_{\log\sigma^2_\alpha},\, s^2_{\log\sigma^2_\alpha}\Big),\\ u_\beta &\sim \mathcal{N}\Big(m_{\log\sigma^2_\beta},\, s^2_{\log\sigma^2_\beta}\Big),\\ u &\sim \mathcal{N}\Big(m_{\log\sigma^2},\, s^2_{\log\sigma^2}\Big). \end{aligned} \tag{16}$$

Samples are generated via:

$$u_\alpha = m_{\log\sigma^2_\alpha} + s_{\log\sigma^2_\alpha}\,\varepsilon_{\sigma_\alpha}, \quad \varepsilon_{\sigma_\alpha} \sim \mathcal{N}(0,1), \tag{17}$$

and then

$$\sigma^2_\alpha = \exp(u_\alpha), \tag{18}$$

with similar expressions for σ^2_β and σ^2. For the group-specific intercepts and slopes, we use a centered parameterization:

$$\alpha_j = \mu_\alpha + \sqrt{\sigma^2_\alpha}\,\varepsilon_{\alpha,j}, \quad \beta_j = \mu_\beta + \sqrt{\sigma^2_\beta}\,\varepsilon_{\beta,j}, \tag{19}$$

where the auxiliary variables have variational distributions

$$q(\varepsilon_{\alpha,j}) = \mathcal{N}\Big(m_{\varepsilon_{\alpha,j}},\, s^2_{\varepsilon_{\alpha,j}}\Big), q(\varepsilon_{\beta,j}) = \mathcal{N}\Big(m_{\varepsilon_{\beta,j}},\, s^2_{\varepsilon_{\beta,j}}\Big). \tag{20}$$

Samples are generated as:

$$\varepsilon_{\alpha,j} = m_{\varepsilon_{\alpha,j}} + s_{\varepsilon_{\alpha,j}}\,\varepsilon'_{\alpha,j}, \quad \varepsilon'_{\alpha,j} \sim \mathcal{N}(0,1), \tag{21}$$

and similarly for $\varepsilon_{\beta,j}$. In a standard (non-incremental) variational inference setting, our goal is to approximate the true posterior

$$p(\theta \mid \boldsymbol{D}) = \frac{p(\theta, \boldsymbol{D})}{p(\boldsymbol{D})} \tag{22}$$

with the variational distribution $q(\theta;\lambda)$. To this end, we minimize the Kullback–Leibler (KL) divergence:

$$\mathrm{KL}\Big(q(\theta;\lambda)\,\|\,p(\theta \mid \boldsymbol{D})\Big) = \int q(\theta;\lambda)\,\log\frac{q(\theta;\lambda)}{p(\theta \mid \boldsymbol{D})}\,d\theta. \tag{23}$$

Substituting $p(\theta \mid \boldsymbol{D}) = \frac{p(\theta,\boldsymbol{D})}{p(\boldsymbol{D})}$, we have:

$$\mathrm{KL}\Big(q(\theta;\lambda)\,\|\,p(\theta \mid \boldsymbol{D})\Big) = \int q(\theta;\lambda)\,\log\frac{q(\theta;\lambda)\,p(\boldsymbol{D})}{p(\theta,\boldsymbol{D})}\,d\theta. \tag{24}$$

Rearrange the terms to obtain:

$$\begin{aligned} \log p(\boldsymbol{D}) &= \mathrm{KL}\Big(q(\theta;\lambda)\,\|\,p(\theta \mid \boldsymbol{D})\Big)\\ &\quad + \int q(\theta;\lambda)\,\log\frac{p(\theta,\boldsymbol{D})}{q(\theta;\lambda)}\,d\theta. \end{aligned} \tag{25}$$

Fig. 2 Target area (32,334 buildings)

we aim to maximize the Evidence Lower Bound (ELBO),

$$\mathcal{L}(\lambda) = \mathbb{E}_{q(\theta;\lambda)}\Big[\log p(\theta,\boldsymbol{D}) - \log q(\theta;\lambda)\Big]. \tag{26}$$

Furthermore,

$$\begin{aligned} \mathcal{L}(\lambda) = &\underbrace{\mathbb{E}_{q(\theta;\lambda)}\big[\log p(\theta)\big]}_{\text{Prior term}} + \underbrace{\mathbb{E}_{q(\theta;\lambda)}\big[\log p(\boldsymbol{D} \mid \theta)\big]}_{\text{Likelihood term}}\\ &- \underbrace{\mathbb{E}_{q(\theta;\lambda)}\big[\log q(\theta;\lambda)\big]}_{\text{Entropy term}}. \end{aligned} \tag{27}$$

Where $\boldsymbol{D} = \{\text{EDP, IM}\}$, practically, one often minimizes its negative by gradient decent. When new data $\boldsymbol{D}_{\text{new}}$ arrives, we use the previous posterior $q_{\text{old}}(\theta)$ as a predictive prior. The online ELBO is then defined as:

$$\begin{aligned} \mathcal{L}_{\text{sequential}} = &\underbrace{\mathbb{E}_{q_t(\theta)}\Big[\log p(\boldsymbol{D}_{\text{new}} \mid x,\,\theta)\Big]}_{\text{New data fit}} + \underbrace{\mathbb{E}_{q_t(\theta)}\Big[\log p_{\text{pred}}(\theta)\Big]}_{\text{Predictive prior}}\\ &- \underbrace{\mathbb{E}_{q_t(\theta)}\Big[\log q_t(\theta)\Big]}_{\text{Entropy term}}. \end{aligned} \tag{28}$$

5. Seismic risk assessment in Sendai city

Based on the parameters of the Nagamachi-Rifu fault and the recipe reported by Irikura (2011)[17], four more specific fault models were generated by varying the original parameters. The magnitudes for the training dataset range from 6.3 to 7.5 based on the Japan Meteorological Agency magnitude scale. Taking into account the uncertainty, 5 different patterns of random phases are applied to these 13 magnitudes, and 7 magnitudes of them are selected as validation sets.

This approach yielded a data set that included peak ground acceleration and maximum inter-story drift angle. Following the principles of POD, spacial modes of peak ground acceleration and maximum inter-story drift angle were obtained and allowed for the calculation of optimal sensor distribution. The obtained result is that a network with a minimum of 5 sensors is optimized for IM (peak ground acceleration), and an optimized distribution network of 6 sensors for EDP (maximum story drift angle) is

found, as shown in Fig.3. Both of each sensor network has reached about 20% of prediction error as shown in Fig.6. Figures 4 and 5 present a comparison between the original simulation results and the prediction results. It can be confirmed that the prediction result fairly well reproduce the simulation result.

Fig. 3 Sensor distribution

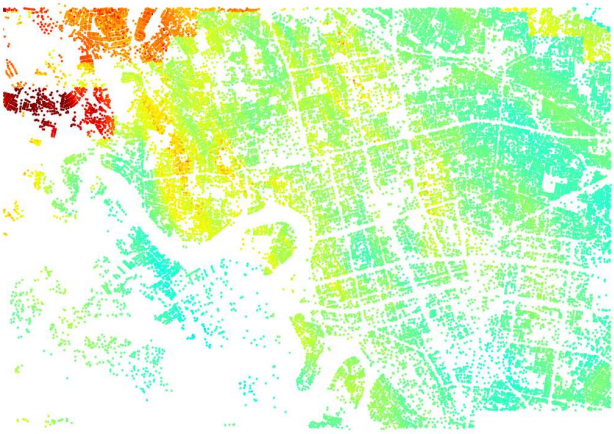

Fig. 4 Simulation result (PGA)

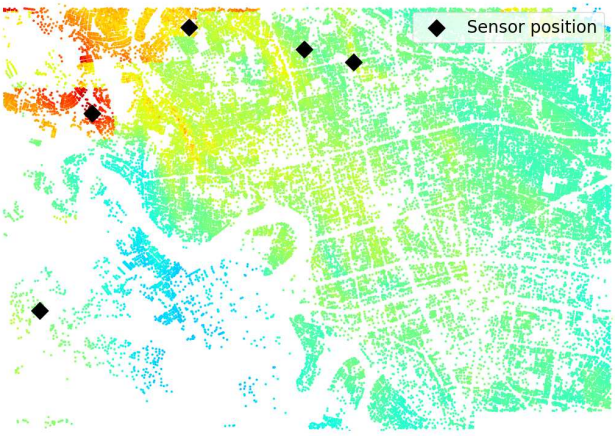

Fig. 5 Prediction result (PGA)

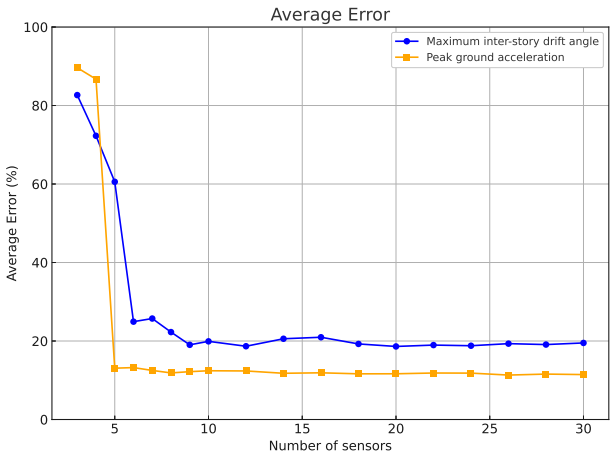

Fig. 6 Error of prediction

Using obtained simulation results, a sparse sensor network was optimized, enabling predictions of ground motion and structural responses within urban areas from limited sensor observations. A data-driven risk assessment model for urban areas was also developed, and the model integrates hierarchical Bayesian modeling and variational inference to estimate complex posterior distributions, enabling sequential updating of seismic risk assessments. The effectiveness of the proposed model was demonstrated through sequential updating using the complete numerical simulation dataset, resulting in updated fragility maps. The sequential updating process, along with corresponding intensity measure (IM) maps and damage probability maps generated from fragility functions for the modeled structural type, is illustrated in Fig. 7. This sequential process ensures that each step reflects the most recent data inputs, providing continuously updated seismic damage assessments within a hierarchical framework that facilitates data integration across urban areas.

6. Conclusion

In this study, numerical simulations were conducted to generate various seismic scenarios by modeling fault models, geological structures, and urban building structures using the Stochastic Green's Function and Integrated Earthquake Simulation (IES). Based on the simulated data, a sparse sensor network was optimized with the help of POD, enabling predictions of ground motion and structural responses within urban areas from limited sensor observations. Additionally, a data-driven risk assessment model for urban areas was developed. This model builds upon the traditional analytical fragility assessment method known as cloud analysis and extends it by incorporating hierarchical Bayesian modeling and variational inference for estimating complex posterior distributions, enabling sequential updating of seismic risk assessments. The proposed model was validated using numerically simulated data and hypothetical sensor network observations, allowing for rapid and sequentially updated seismic damage assessments within a hierarchical framework that facilitates

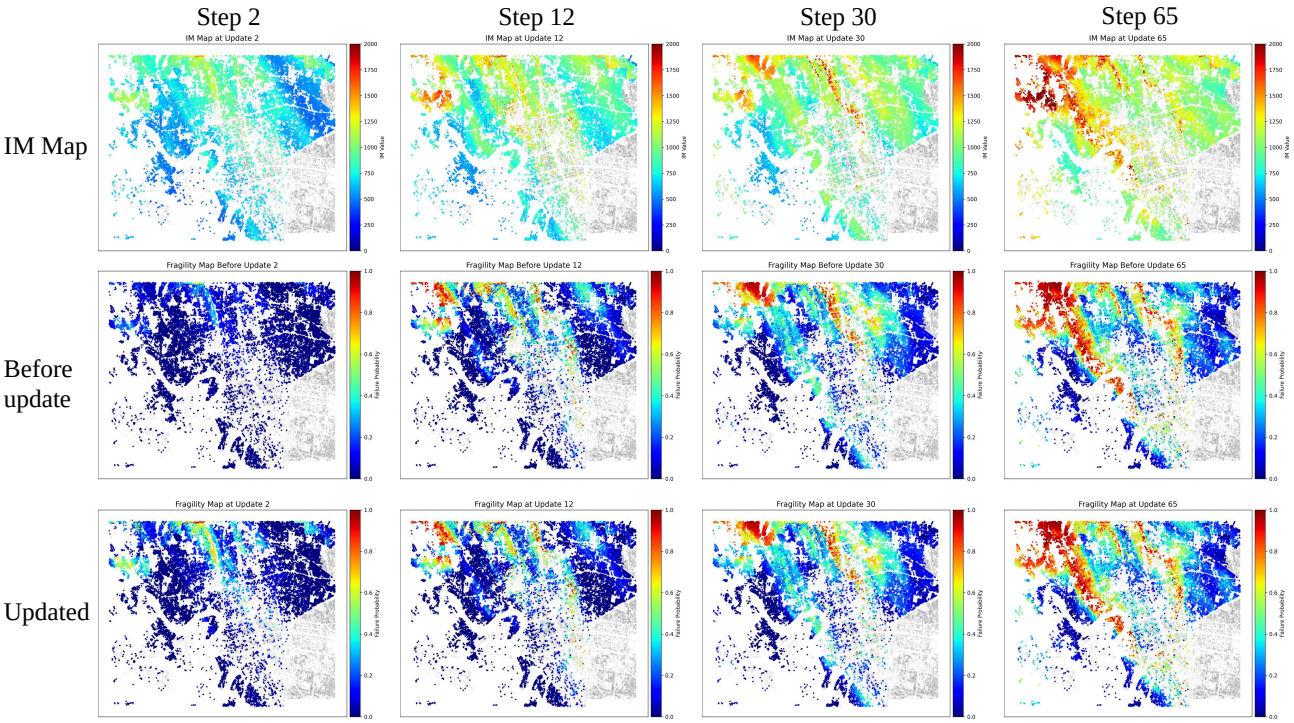

Fig. 7 IM maps and damage probability maps obtained from fragility functions

data integration across urban areas.

REFERENCES

[1] Irikura, K.: Prediction of strong acceleration motion using empirical Green's function, Proc. 7th Japan Earthq. Eng. Symp., vol. 151, 1986.

[2] Irikura, Kojiro: Prediction of strong acceleration motion using empirical Green's function, Proc. 7th Japan Earthq. Eng. Symp., vol. 151, pp. 151-156, 1986.

[3] Dan, K. and Sato, T.: Strong-motion prediction by semi-empirical method based on variable-slip rupture model of earthquake fault; J. Struct. Constr. Eng., AIJ, No.509, pp. 49-60, 1998

[4] National Research Institute for Earth Science and Disaster Resilience: J-SHIS Earthquake Hazard Station, 2011. Available from: https://www.j-shis.bosai.go.jp/.

[5] Hori, M.: Introduction to computational earthquake engineering, Imperial College Press, 2011.

[6] Liang, Y. C., et al.: Proper orthogonal decomposition and its applications—Part I: Theory, Journal of Sound and Vibration, Vol. 252, No. 3, pp. 527-544, 2002.

[7] Nakai, K., Yamada, et al.: Effect of Objective Function on Data-Driven Greedy Sparse Sensor Optimization, in IEEE Access, Vol. 9, pp. 46731-46743, 2022.

[8] Saouma, V.E., Hariri-Ardebili, M.A.: Fragility Functions, In Aging, Shaking, and Cracking of Infrastructures, Springer, Cham, 2021.

[9] Padgett, Jamie E., and DesRoches, Reginald., et al: Selection of optimal intensity measures in probabilistic seismic demand models of highway bridge portfolios, Earthquake Engineering & Structural Dynamics, Vol. 37, No. 5, pp. 711-725, 2008.

[10] Li, Jian and Spencer, Billie F., et al.: Bayesian Updating of Fragility Functions Using Hybrid Simulation, Journal of Structural Engineering, Vol. 139, No. 7, pp. 1160-1171, 2013.

[11] Koutsourelakis, Phadeon-Stelios: Assessing structural vulnerability against earthquakes using multi-dimensional fragility surfaces: A Bayesian framework, Probabilistic Engineering Mechanics, Vol. 25, No. 1, pp. 49-60, Elsevier, 2010.

[12] FEMA: Hazus-MH 2.1 technical manual: Earthquake model, Federal Emergency Management Agency, Mitigation Division, Washington, DC, 2012.

[13] Gelman, A., Carlin, J., et al.: Chapter 15 Hierarchical linear models, Bayesian Data Analysis, 3rd ed., Chapman and Hall/CRC, pp. 381–402, 2013.

[14] Gelman, Andrew and Hill, Jennifer., et al.: Data Analysis Using Regression and Multilevel/Hierarchical Models, Cambridge University Press, 2007.

[15] Hoffman, M. D., Blei, D. M., Wang, C., Paisley, J.: Stochastic Variational Inference, Journal of Machine Learning Research, Vol. 14, pp. 1303–1347, 2013.

[16] Blei, D. M., Kucukelbir, A., McAuliffe, J. D.: Variational Inference: A Review for Statisticians, Journal of the American Statistical Association, Vol. 112, No. 518, pp. 859–877, 2017.

[17] Irikura, K., Hiroe, M.: Recipe for Predicting Strong Ground Motion from Crustal Earthquake Scenarios, Pure and Applied Geophysics, Vol. 168, No. 1, pp. 85-104, 2011.